

# Generation of Circularly Polarized High Harmonics with Identical Helicity in Two-Dimensional Materials

Navdeep Rana,<sup>1</sup> M. S. Mrudul,<sup>2</sup> and Gopal Dixit<sup>1,\*</sup>

<sup>1</sup>*Department of Physics, Indian Institute of Technology Bombay, Powai, Mumbai 400076, India*

<sup>2</sup>*Department of Physics and Astronomy, Uppsala University, P.O. Box 516, SE 75120 Uppsala, Sweden*



(Received 11 July 2022; accepted 21 November 2022; published 16 December 2022)

Generation of circularly polarized high harmonics with the same helicity to all orders is indispensable for chiral-sensitive spectroscopy with attosecond temporal resolution. Solid-state samples have added a valuable asset in controlling the polarization of emitted harmonics. However, maintaining the identical helicity of the emitted harmonics to all orders is a daunting task. In this work, we demonstrate a robust recipe for efficient generation of circularly polarized harmonics with the same helicity. For this purpose, a nontrivial tailored driving field, consisting of two co-rotating laser pulses with frequencies  $\omega$  and  $2\omega$ , is utilized to generate harmonics from graphene. The Lissajous figure of the total driving pulse exhibits an absence of rotational symmetry, which imposes no constraint on the helicity of the emitted harmonics. Our approach to generating circularly polarized harmonics with the same helicity is robust against various perturbations in the setup, such as variation in the subcycle phase difference or the intensity ratio of the  $\omega$  and  $2\omega$  pulses, as rotational symmetry of the total driving pulse remains absent. Our approach is expected to be equally applicable to other two-dimensional materials, among others, transition-metal dichalcogenides and hexagonal boron nitride, as our approach is based on the absence of rotational symmetry of the driving pulse. Our work paves the way for establishing compact solid-state chiral extreme ultraviolet sources, opening a realm for chiral light-matter interaction on its intrinsic timescale.

DOI: 10.1103/PhysRevApplied.18.064049

## I. INTRODUCTION

In the last few decades, high-harmonic generation (HHG) has become an essential ingredient in attosecond science. HHG is a strong-field-driven highly nonlinear frequency up-conversion process. HHG provides a route not only to generate attosecond pulses in the extreme ultraviolet (XUV) energy regime [1] but also to interrogate electron dynamics on its natural timescale [2–5]. Owing to the recollision mechanism of HHG in gases [6], the harmonic yield drops markedly as the polarization of the driving laser pulse changes from linear to circular. To circumvent this problem, a combination of two counter-rotating circularly polarized laser pulses with frequencies  $\omega$  and  $2\omega$  has been employed to generate circularly-polarized harmonics. The resultant harmonic spectrum displays doublets of circularly polarized harmonics where  $(3n + 1)$  and  $(3n + 2)$  harmonics exhibit the polarization of  $\omega$  and  $2\omega$  fields, respectively. However,  $3n$  harmonics do not conserve parity and thus they are forbidden [7,8]. Different variants of the bichromatic counter-rotating  $\omega$ - $2\omega$  schemes, such as varying the ratio of the ellipticities and/or of the intensities of the two driving pulses [9,10],

controlling the subcycle phase between the two pulses [11], introduction of an additional seed pulse with different polarization [12,13], adding plasmonic field enhancement [14], and noncollinear geometry of the  $\omega$ - $2\omega$  scheme [15,16], are employed to control the polarization of the emitted harmonics. It is important to emphasize that the recognition of chiral molecules [17,18], circular dichroism in magnetic materials [19], spin and magnetization dynamics in solids at their natural timescales [20,21], to name but a few, are examples of chiral-sensitive light-matter interaction phenomena where the desired control over the polarization of the emitted harmonics and resultant attosecond XUV pulses is quintessential.

The extension of HHG from gases to solids offers an attractive option for compact tabletop sources of coherent XUV attosecond pulses. Because of the periodic nature of solids with higher electron density in comparison with gases, HHG in solids seems a better option for higher yield of harmonics [22,23]. Moreover, solid HHG has added a further dimension in attosecond spectroscopy to shed light on various equilibrium and nonequilibrium aspects of solids [24–39]. In comparison with HHG from gases, HHG from solids exhibits different sensitivity toward circularly-polarized laser pulses [40,41]. It has been shown that a high degree of control over the polarization of emitted

\*gdixit@phy.iitb.ac.in

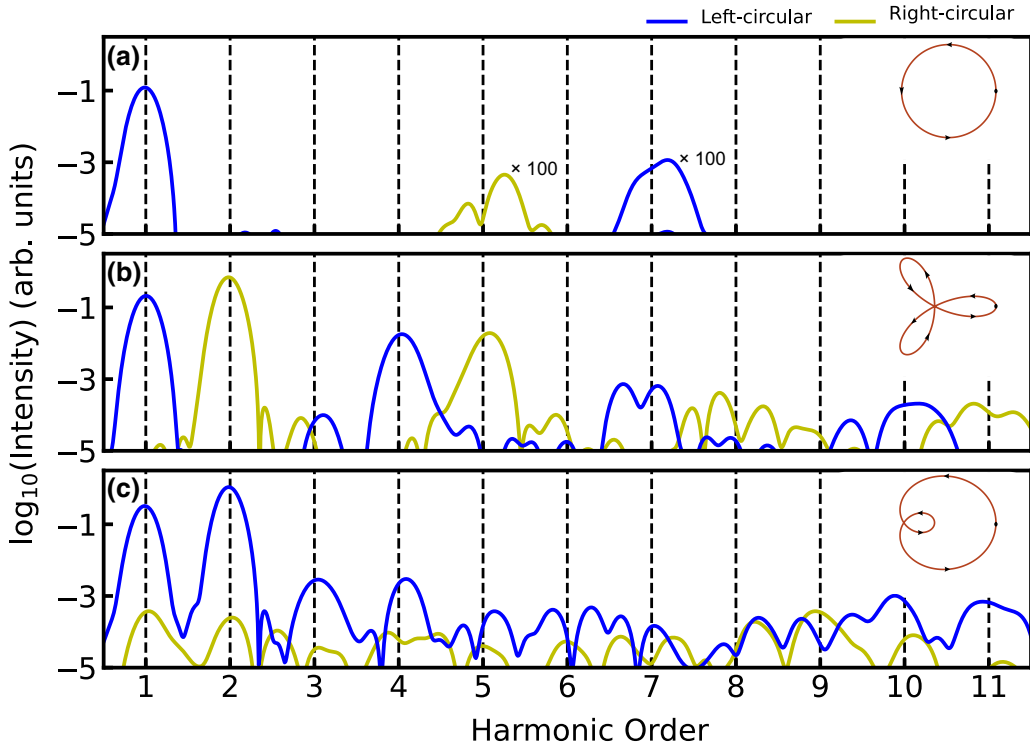


FIG. 1. Polarization-resolved high-harmonic spectrum of graphene driven by (a) single-color circularly polarized, (b) bicircular counter-rotating  $\omega$ - $2\omega$ , and (c) bicircular co-rotating  $\omega$ - $2\omega$  laser pulses. In all cases, the fundamental  $\omega$  pulse is left-handed polarized. Lissajous figures of the total driving fields are shown in the respective insets. In all cases, the peak intensity of the  $\omega$  pulse is 0.3 TW/cm<sup>2</sup> and the wavelength is 2  $\mu$ m. The subcycle phase difference between the two pulses  $\phi$  is zero, and the relative strength of the electric fields between  $\omega$  and  $2\omega$  pulses  $R$  is 2 in (b),(c).

harmonics can be achieved by the dynamic control of crystal symmetries and intertwined interband and intraband electronic dynamics [42]. Saito *et al.* have demonstrated the generation of harmonics with alternate helicity using a circularly polarized laser pulse, owing to the selection rules derived from the symmetry [43]. Recently, bicircular counter-rotating  $\omega$ - $2\omega$  laser pulses have been employed to generate circularly polarized harmonics in solids, which has enabled one to perform symmetry-resolved chiral spectroscopy [44] and to probe valley-selective excitations in two-dimensional materials [45–47]. In all cases, the harmonic spectra of solids, similar to gases, are composed of pairs of circularly polarized harmonics with opposite helicity owing to the threefold rotational symmetry of the bicircular counter-rotating pulses. Thus, the generation of circularly polarized harmonics with the same helicity to all orders is missing—a major impediment in the realization of a compact all-solid-state XUV source for chiral spectroscopy. The main focus of the present work is to address this major obstacle.

Our work provides a robust recipe to generate circularly-polarized harmonics with the same helicity to all orders. For that purpose, a nontrivial tailored driving field without any rotational symmetry is designed for HHG.

The total electric field of the co-rotating bicircular  $\omega$ - $2\omega$  pulses does not exhibit any symmetry, which is in contrast to the counter-rotating  $\omega$ - $2\omega$  pulses with threefold symmetry. Thus, it is expected that the absence of any symmetry of the total driving field will impose no symmetry constraint on the helicity of the emitted harmonics. To test our idea, monolayer graphene is exposed to a combination of bicircular co-rotating  $\omega$ - $2\omega$  laser pulses. It is worth mentioning that HHG from graphene and the underlying mechanism have been extensively explored in recent years [48–57]. Moreover, the anomalous ellipticity dependence of HHG from graphene has been explored experimentally [54,58] as well as discussed theoretically [53,54,58–61].

## II. COMPUTATIONAL DETAILS

Semiconductor Bloch equations in the Houston basis are solved to simulate the interaction of laser with graphene. The nearest-neighbor tight-binding approach is used to represent graphene as discussed in our previous work [62]. High-harmonic spectrum is simulated by performing the Fourier transform ( $\mathcal{FT}$ ) of the time derivative of the total

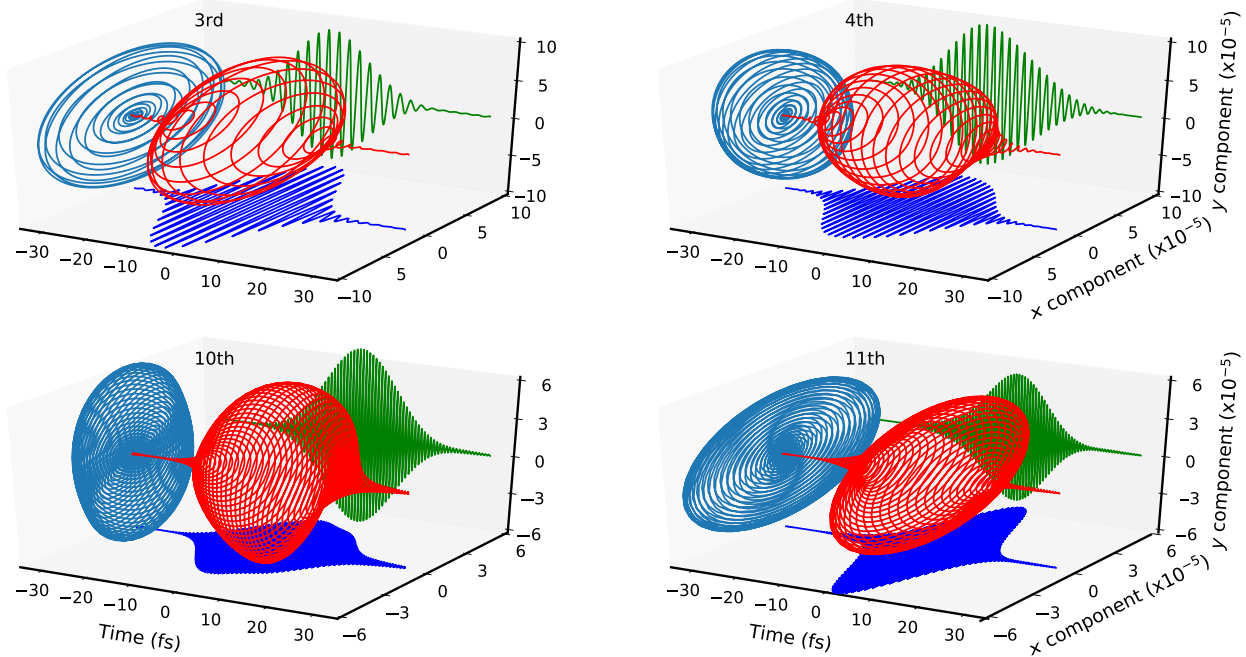


FIG. 2. Time profiles of the emitted harmonics, shown in Fig. 1(c), generated by bicircular co-rotating  $\omega$ - $2\omega$  laser pulses (red color). The  $x$  and  $y$  components of the harmonics are shown in blue and green colors, respectively. The Lissajous figures of the emitted harmonics are shown in cyan color. All harmonics are left-handed circularly polarized. The ellipticities of the 3rd, 4th, 10th, and 11th harmonics are 0.8, 0.8, 0.8, and 0.9, respectively.

current as

$$\mathcal{I}(\omega) = \left| \mathcal{FT} \left( \frac{d}{dt} \left[ \int_{BZ} \mathbf{J}(\mathbf{k}, t) d\mathbf{k} \right] \right) \right|^2. \quad (1)$$

Here,  $\mathbf{J}(\mathbf{k}, t)$  is the current at any  $\mathbf{k}$ -point in the Brillouin zone as a function of time.

### III. RESULTS AND DISCUSSION

Before we discuss results obtained for bicircular co-rotating  $\omega$ - $2\omega$  laser pulses, let us revisit the results for single-color and bicircular counter-rotating  $\omega$ - $2\omega$  laser pulses. The polarization-resolved high-harmonic spectrum of graphene driven by a single-color left-handed circularly-polarized pulse is shown in Fig. 1(a). Owing to the sixfold rotational symmetry of graphene and conservation of spin angular momentum of the driving laser pulse, selection rules indicate the generation of  $(6n \pm 1)$ -order harmonics with  $n = 0, 1, 2, 3, \dots$ . Moreover, the helicity of the  $6n + 1$  ( $6n - 1$ ) harmonics is the same (opposite) helicity as the driving pulse [63]. Our results in Fig. 1(a) are in perfect agreement with the selection rules and with an earlier report [55]. Moreover, the low harmonic yield of the fifth and seventh harmonics with opposite helicity has been observed in an experiment [58]. It has been anticipated that the yield of harmonics can be improved by increasing the intensity of the driving field [55].

The total vector potential corresponding to  $\omega$ - $2\omega$  circularly polarized laser pulses is given as

$$\mathbf{A}(t) = \frac{A_0 f(t)}{\sqrt{2}} \left( \left[ \cos(\omega t + \phi) + \frac{R}{2} \cos(2\omega t) \right] \hat{\mathbf{e}}_x + \left[ \sin(\omega t + \phi) \pm \frac{R}{2} \sin(2\omega t) \right] \hat{\mathbf{e}}_y \right). \quad (2)$$

Here,  $A_0$  is the amplitude of the vector potential,  $f(t)$  is the temporal envelope of the driving field,  $\phi$  is the subcycle phase difference between  $\omega$  and  $2\omega$  pulses, and  $R$  is the ratio of electric field strength of the two pulses.  $+$  ( $-$ ) represents the co-rotating (counter-rotating) laser pulse configuration. In this work, a fundamental  $\omega$  pulse with a peak intensity of 0.3 TW/cm<sup>2</sup> and a wavelength of 2  $\mu$ m is used for HHG from graphene. The fundamental driving pulse has eight cycles with sin-square envelope. Similar laser parameters have been employed to study coherent electron dynamics in graphene [64,65].

Figure 1(b) presents the polarization-resolved harmonic spectrum of graphene driven by bicircular counter-rotating  $\omega$ - $2\omega$  laser pulses. The resultant vector potential exhibits a trefoil symmetry as shown in the inset. Following the threefold symmetry and conservation of spin angular momentum,  $n\omega = p\omega + 2q\omega$  with  $p = q \pm 1$  harmonics are allowed, whereas  $3n$  harmonics are symmetry forbidden [8].  $p$  ( $q$ ) is the number of photons of the  $\omega$  ( $2\omega$ ) pulse.

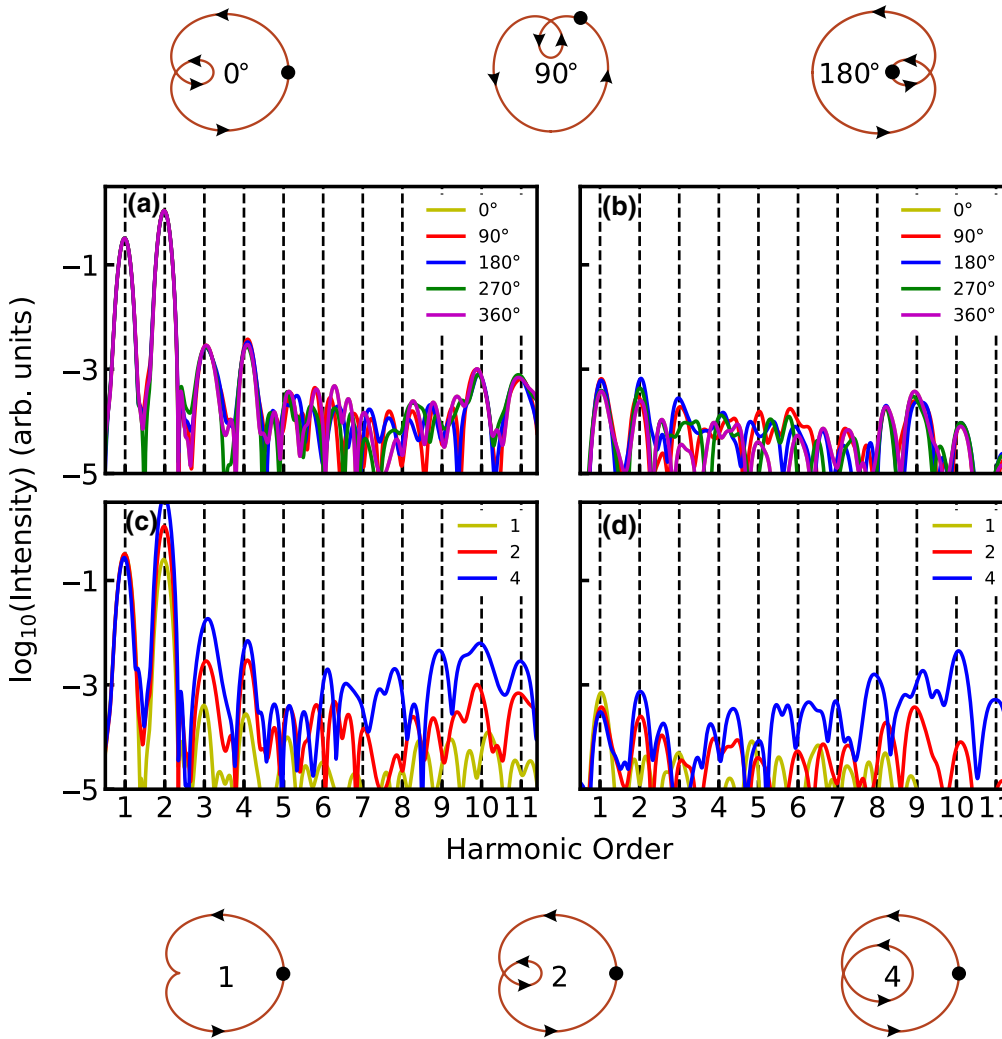


FIG. 3. High-harmonic spectra of graphene driven by bicircular co-rotating  $\omega$ - $2\omega$  laser pulses for different values of (a),(b) the subcycle phases  $\phi$  and (c),(d) the relative electric field strengths  $R$ . Left- and right-hand panels show the contributions of left- and right-handed polarization to the harmonics, respectively. Lissajous figures of the resultant vector potential, associated with bicircular co-rotating  $\omega$ - $2\omega$  laser pulses, are shown above and below the panels for different values of  $\phi$  and  $R$ , respectively. The  $x$  and  $y$  components of the total vector potential as given in Eq. (2) are plotted omitting the envelope function along the  $X$  and  $Y$  axes for different values of  $\phi$  and  $R$  as mentioned in the inset. These inset plots are aimed to display the symmetry of the total field corresponding to different phase and intensity relations between  $\omega$  and  $2\omega$  fields. The black dot in each Lissajous figure corresponds to the start of the vector potential at  $t = 0$ .

Moreover, the allowed  $(3n + 1)$ - and  $(3n + 2)$ -order harmonics follow the helicity of the  $\omega$  and  $2\omega$  pulses, respectively [19,44,45]. From the figure, our results are consistent with the selection rules and an earlier report [46]. Note that the polarization of one of the driving pulses individually impacts the helicity of the emitted harmonics significantly.

Analysis of results in Figs. 1(a) and 1(b) establishes that the generation of harmonics with circular polarization, using either a single-color circular pulse or bicircular counter-rotating  $\omega$ - $2\omega$  pulses, is possible. In both cases, the adjacent harmonics are of opposite helicity, which has a serious consequence for the helicity of the resultant attosecond pulses. If the intensities of adjacent harmonics with opposite helicity are the same then the generated attosecond pulse exhibits linear polarization with a rotating axis of polarization. In such circumstances, one needs to induce an imbalance in the intensity of the adjacent harmonics to have a control over the helicity of the resultant attosecond pulses [10–12].

The total harmonic spectrum in polarization-resolved fashion for the bicircular co-rotating  $\omega$ - $2\omega$  laser pulses

is presented in Fig. 1(c). As evident from the Lissajous figure in the inset, the total field does not exhibit any rotational symmetry. Thus, the conservation of spin angular momentum does not impose any constraint on the helicity of the generated harmonics and none of the harmonics are symmetry forbidden. As a result, all-order circularly-polarized harmonics are generated with the same helicity as that of the driving pulse. Analysis of the relative yield of the spectrum reveals that the left-circularly polarized harmonics are the leading harmonics.

After demonstrating the capability of the co-rotating  $\omega$ - $2\omega$  scheme to generate circularly polarized harmonics with the same helicity, let us analyze the temporal evolution of the emitted harmonics in the time domain. For this purpose, Fig. 2 presents the time profiles of a few selected harmonics corresponding to Fig. 1(c). All the harmonics are left-handed circularly polarized as evident from the Lissajous figure and the  $x$  and  $y$  components of the harmonics in the time domain.

At this juncture it is natural to wonder how robust are the features of the spectrum shown in Fig. 1(c) with respect to

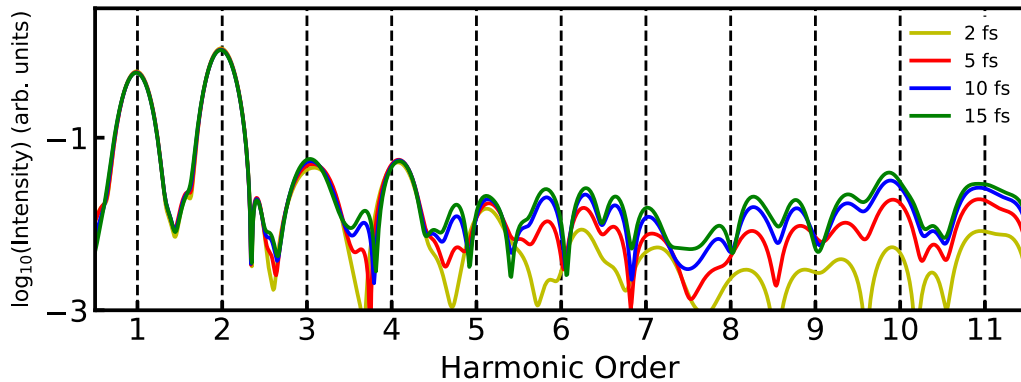


FIG. 4. High-harmonic spectrum of graphene generated by bicircular co-rotating  $\omega$ - $2\omega$  laser pulses for different values of dephasing time. Helicity of the emitted harmonics is the same as that of the  $\omega$  driving pulse, i.e., left-handed circularly polarized. The laser parameters are the same as those used in Fig. 1(c).

the variations in the subcycle phase  $\phi$  and the relative ratio  $R$ . To avoid overlapping and have a better representation, we present the harmonics with left- and right-handed circular polarization in the left- and right-hand panels of Fig. 3, respectively. Figures 3(a) and 3(b) display the harmonic spectrum for different values of  $\phi$ . From the figure, the polarization state of the emitted harmonics is insensitive with respect to variations in  $\phi$ , and all the harmonics are left-handed circularly polarized in nature. To understand the insensitivity, let us look at the total electric field of the co-rotating  $\omega$ - $2\omega$  scheme for different values of  $\phi$  as shown above the panels. As evident from the Lissajous figures of the total field, the variation in  $\phi$  results in the rotation of the resultant field. However, the fields have no rotation symmetry. Thus, there are no significant changes in the polarization and the intensity of the emitted harmonics [see Figs. 3(a) and 3(b)].

Now let us explore how the variation in the  $R$  value affects the harmonic spectra. The peak intensity of the resultant field is maintained at  $0.3 \text{ TW/cm}^2$  while varying the  $R$  value. As expected, an increase in the  $R$  value results in an increase of the harmonic yield [see Figs. 3(c) and 3(d)]. However, the overall nature of the spectra does not change with respect to  $R$ , i.e., harmonics are still circularly polarized in the direction of the driving field. The reason for that can be attributed to the similar Lissajous figures of the resultant field for different  $R$  values as evident from the bottom panel. Thus, the investigation of Fig. 3 leads us to conclude that the generation of circularly polarized harmonics with same helicity via the co-rotating  $\omega$ - $2\omega$  scheme does not require fine tuning of subcycle phase  $\phi$  or intensity ratio  $R$  between the pulses. Therefore, the co-rotating scheme is robust in generating circularly polarized harmonics with the same helicity to all orders.

Before making a summary, let us examine how the harmonic spectrum is sensitive to the dephasing time—a phenomenological term accounting for the decoherence between electrons and holes within the semiconductor Bloch equations framework. Figure 4 presents how the different values of the dephasing time affect the harmonic spectrum corresponding to co-rotating  $\omega$ - $2\omega$  laser pulses. As evident from the figure, lower-order harmonics are

insensitive to the dephasing time as they are dominated by the intraband current [54,62,66]. On the other hand, higher-order harmonics are dominated by the interband current as their intensities are boosted with an increase in the dephasing time. The interband channel is prone to the coherence between the excited electrons and their corresponding holes [54]. Also, longer electron-hole trajectories are sensitive to the decoherence time as the corresponding excursion time allows for more scattering events during HHG [66]. Thus, relatively smaller dephasing time means more scattering events for the same excursion time. Hence, the yield of higher harmonics will be suppressed for smaller dephasing time [66]. Note that the increase in the harmonic yield with increase of dephasing time does not alter the polarization properties of the emitted harmonics as evident from Fig. 4.

#### IV. CONCLUSION

In summary, we explore the possibility of generating circularly polarized high harmonics with the same helicity in solids. To achieve this goal, we harness the no rotational symmetry of the tailored driving field consisting of two co-rotating circular pulses with frequencies  $\omega$  and  $2\omega$ . The absence of rotational symmetry of the driving field enforces no constraint on the helicity of the emitted harmonics. It is observed that the spectrum of monolayer graphene, driven by the bicircular co-rotating pulses, consists of circularly polarized harmonics with the same helicity to all orders as that of the fundamental  $\omega$  pulse. The Lissajous figure of the total driving pulse exhibits no rotational symmetry for different subcycle phase differences between  $\omega$  and  $2\omega$  pulses and different intensity ratios between the pulses. Moreover, dephasing time, associated with the decoherence between electrons and holes, does not alter the nature of the harmonic spectrum. Thus, our approach for generating circularly polarized high harmonics with the same helicity is robust against any imperfection in the driving pulses. Furthermore, we anticipate that our approach will be applicable to other hexagonal two-dimensional materials, such as hexagonal boron nitride and molybdenum disulfide, as our approach is based on the

absence of rotational symmetry of the total system consisting of the total driving field and the two-dimensional material. However, unlike gapless graphene, the interplay of the interband and intraband currents is different in gapped graphene [67], and therefore the value of the dephasing time will play a crucial role in determining the helicity of the emitted harmonics in gapped graphene. Thus, laser parameters need to be optimized to obtain a desired control over the helicity of the emitted harmonics from gapped graphene. Also, based on the results presented in Ref. [44], our approach could be extended to bulk materials. The present work offers an avenue for detailed chiral-sensitive light-matter interactions on natural timescales.

## ACKNOWLEDGMENTS

G.D. acknowledges support from Science and Engineering Research Board (SERB) India (Project No. MTR/2021/000138).

- [1] Katsumi Midorikawa, Progress on table-top isolated attosecond light sources, *Nat. Photonics* **16**, 267 (2022).
- [2] F. Krausz and M. Ivanov, Attosecond physics, *Rev. Mod. Phys.* **81**, 163 (2009).
- [3] P. H. Bucksbaum, The future of attosecond spectroscopy, *Science* **317**, 766 (2007).
- [4] P. B. Corkum and F. Krausz, Attosecond science, *Nat. Phys.* **3**, 381 (2007).
- [5] G. Dixit, O. Vendrell, and R. Santra, Imaging electronic quantum motion with light, *Proc. Natl. Acad. Sci. USA* **109**, 11636 (2012).
- [6] Paul B. Corkum, Plasma Perspective on Strong Field Multiphoton Ionization, *Phys. Rev. Lett.* **71**, 1994 (1993).
- [7] Ofer Neufeld, Daniel Podolsky, and Oren Cohen, Floquet group theory and its application to selection rules in harmonic generation, *Nat. Commun.* **10**, 1 (2019).
- [8] A. Fleischer, O. Kfir, T. Diskin, P. Sidorenko, and O. Cohen, Spin angular momentum and tunable polarization in high-harmonic generation, *Nat. Photonics* **8**, 543 (2014).
- [9] O. Neufeld and O. Cohen, Optical Chirality in Nonlinear Optics: Application to High Harmonic Generation, *Phys. Rev. Lett.* **120**, 133206 (2018).
- [10] K. M. Dorney, J. L. Ellis, C. Hernández-García, D. D. Hickstein, C. A. Mancuso, N. Brooks, T. Fan, G. Fan, D. Zusin, C. Gentry, P. Grychtol, H. C. Kapteyn, and M. M. Murnane, Helicity-Selective Enhancement and Polarization Control of Attosecond High Harmonic Waveforms Driven by Bichromatic Circularly Polarized Laser Fields, *Phys. Rev. Lett.* **119**, 063201 (2017).
- [11] M. V. Frolov, N. L. Manakov, A. A. Minina, N. V. Vvedenskii, A. A. Silaev, M. Yu Ivanov, and A. F. Starace, Control of Harmonic Generation by the Time Delay Between Two-Color, Bicircular Few-Cycle Mid-IR Laser Pulses, *Phys. Rev. Lett.* **120**, 263203 (2018).
- [12] G. Dixit, Á. Jiménez-Galán, L. Medišauskas, and M. Ivanov, Control of the helicity of high-order harmonic radiation using bichromatic circularly polarized laser fields, *Phys. Rev. A* **98**, 053402 (2018).
- [13] Rambabu Rajpoot, Amol R. Holkundkar, and Jayendra N. Bandyopadhyay, Polarization control of attosecond pulses using bi-chromatic elliptically polarized laser, *J. Phys. B* **54**, 225401 (2021).
- [14] Irfana N. Ansari, Cornelia Hofmann, Lukas Medišauskas, Maciej Lewenstein, Marcelo F. Ciappina, and Gopal Dixit, Controlling polarization of attosecond pulses with plasmonic-enhanced bichromatic counter-rotating circularly polarized fields, *Phys. Rev. A* **103**, 013104 (2021).
- [15] P. C. Huang, C. Hernández-García, J. T. Huang, P. Y. Huang, C. H. Lu, L. Rego, D. D. Hickstein, J. L. Ellis, A. Jaron-Becker, and A. Becker, *et al.*, Polarization control of isolated high-harmonic pulses, *Nat. Photonics* **12**, 349 (2018).
- [16] D. D. Hickstein, F. J. Dollar, P. Grychtol, J. L. Ellis, R. Knut, C. Hernández-García, D. Zusin, C. Gentry, J. M. Shaw, and T. Fan, *et al.*, Non-collinear generation of angularly isolated circularly polarized high harmonics, *Nat. Photonics* **9**, 743 (2015).
- [17] A. Ferré, C. Handschin, M. Dumergue, F. Burgy, A. Comby, D. Descamps, B. Fabre, G. A. Garcia, R. Géneaux, L. Merceron, E. Mével, L. Nahon, S. Petit, B. Pons, D. Staedter, S. Weber, T. Ruchon, V. Blanchet, and Y. Y. Mairesse, A table-top ultrashort light source in the extreme ultraviolet for circular dichroism experiments, *Nat. Photonics* **9**, 93 (2015).
- [18] R. Cireasa, A. E. Boguslavskiy, B. Pons, M. C. H. Wong, D. Descamps, S. Petit, H. Ruf, N. Thiré, A. Ferré, J. Suarez, J. Higuet, B. E. Schmidt, A. F. Alharbi, F. Legare, V. Blanchet, B. Fabre, S. Patchkovskii, O. Smirnova, Y. Mairesse, and V. R. Bhardwaj, Probing molecular chirality on a sub-femtosecond timescale, *Nat. Phys.* **11**, 654 (2015).
- [19] O. Kfir, P. Grychtol, E. Turgut, R. Knut, D. Zusin, D. Popmintchev, T. Popmintchev, H. Nembach, J. M. Shaw, A. Fleischer, H. Kapteyn, M. Murnane, and O. Cohen, Generation of bright phase-matched circularly-polarized extreme ultraviolet high harmonics, *Nat. Photonics* **9**, 99 (2015).
- [20] C. Boeglin, E. Beaurepaire, V. Halté, V. López-Flores, C. Stamm, N. Pontius, H. A. Dürr, and J. Y. Bigot, Distinguishing the ultrafast dynamics of spin and orbital moments in solids, *Nature* **465**, 458 (2010).
- [21] I. Radu, K. Vahaplar, C. Stamm, T. Kachel, N. Pontius, H. A. Dürr, T. A. Ostler, J. Barker, R. F. L. Evans, R. W. Chantrell, A. Tsukamoto, A. Itoh, A. Kirilyuk, T. Rasing, and A. V. Kimel, Transient ferromagnetic-like state mediating ultrafast reversal of antiferromagnetically coupled spins, *Nature* **472**, 205 (2011).
- [22] Eleftherios Goulielmakis and Thomas Brabec, High harmonic generation in condensed matter, *Nat. Photonics* **16**, 411 (2022).
- [23] S. Ghimire and D. A. Reis, High-harmonic generation from solids, *Nat. Phys.* **15**, 10 (2019).
- [24] Amar Bharti, M. S. Mrudul, and Gopal Dixit, High-harmonic spectroscopy of light-driven nonlinear anisotropic anomalous Hall effect in a Weyl semimetal, *Phys. Rev. B* **105**, 155140 (2022).

- [25] Adhip Pattanayak, Sumiran Pujari, and Gopal Dixit, Role of Majorana fermions in high-harmonic generation from Kitaev chain, *Sci. Rep.* **12**, 1 (2022).
- [26] Ben Zaks, Ren-Bao Liu, and Mark S. Sherwin, Experimental observation of electron–hole recollisions, *Nature* **483**, 580 (2012).
- [27] T. T. Luu, M. Garg, S.Yu. Kruchinin, A. Moulet, M.Th. Hassan, and E. Goulielmakis, Extreme ultraviolet high-harmonic spectroscopy of solids, *Nature* **521**, 498 (2015).
- [28] O. Schubert, M. Hohenleutner, F. Langer, B. Urbanek, C. Lange, U. Hettner, D. Golde, T. Meier, M. Kira, S. W. Koch, and R. Huber, Sub-cycle control of terahertz high-harmonic generation by dynamical Bloch oscillations, *Nat. Photonics* **8**, 119 (2014).
- [29] M. Hohenleutner, F. Langer, O. Schubert, M. Knorr, U. Hettner, S. W. Koch, M. Kira, and R. Huber, Real-time observation of interfering crystal electrons in high-harmonic generation, *Nature* **523**, 572 (2015).
- [30] Adhip Pattanayak, M. S. Mrudul, and Gopal Dixit, Influence of vacancy defects in solid high-order harmonic generation, *Phys. Rev. A* **101**, 013404 (2020).
- [31] G. Vampa, T. J. Hammond, N. Thiré, B. E. Schmidt, F. Légaré, C. R. McDonald, T. Brabec, and P. B. Corkum, Linking high harmonics from gases and solids, *Nature* **522**, 462 (2015).
- [32] G. Vampa, T. J. Hammond, N. Thiré, B. E. Schmidt, F. Légaré, C. R. McDonald, T. Brabec, D. D. Klug, and P. B. Corkum, All-Optical Reconstruction of Crystal Band Structure, *Phys. Rev. Lett.* **115**, 193603 (2015).
- [33] Fabian Langer, Christoph P. Schmid, Stefan Schlauderer, Martin Gmitra, Jaroslav Fabian, Philipp Nagler, Christian Schüller, Tobias Korn, P. G. Hawkins, and J. T. Steiner, *et al.*, Lightwave valleytronics in a monolayer of tungsten diselenide, *Nature* **557**, 76 (2018).
- [34] T. T. Luu and H. J. Wörner, Measurement of the Berry curvature of solids using high-harmonic spectroscopy, *Nat. Commun.* **9**, 1 (2018).
- [35] Hunter B. Banks, Qile Wu, Darren C. Valovcin, Shawn Mack, Arthur C. Gossard, Loren Pfeiffer, Ren-Bao Liu, and Mark S. Sherwin, Dynamical Birefringence: Electron-Hole Recollisions as Probes of Berry Curvature, *Phys. Rev. X* **7**, 041042 (2017).
- [36] M. S. Mrudul, A. Pattanayak, M. Ivanov, and G. Dixit, Direct numerical observation of real-space recollision in high-order harmonic generation from solids, *Phys. Rev. A* **100**, 043420 (2019).
- [37] S. Imai, A. Ono, and S. Ishihara, High Harmonic Generation in a Correlated Electron System, *Phys. Rev. Lett.* **124**, 157404 (2020).
- [38] M. Borsch, C. P. Schmid, L. Weigl, S. Schlauderer, N. Hoffmann, C. Lange, J. T. Steiner, S. W. Koch, R. Huber, and M. Kira, Super-resolution lightwave tomography of electronic bands in quantum materials, *Science* **370**, 1204 (2020).
- [39] Navdeep Rana, M. S. Mrudul, Daniil Kartashov, Misha Ivanov, and Gopal Dixit, High-harmonic spectroscopy of coherent lattice dynamics in graphene, *Phys. Rev. B* **106**, 064303 (2022).
- [40] S. Ghimire, A. D. DiChiara, E. Sistrunk, P. Agostini, L. F. DiMauro, and D. A. Reis, Observation of high-order harmonic generation in a bulk crystal, *Nat. Phys.* **7**, 138 (2011).
- [41] Nicolas Tancogne-Dejean, Oliver D. Mücke, Franz X. Kärtner, and Angel Rubio, Ellipticity dependence of high-harmonic generation in solids originating from coupled intraband and interband dynamics, *Nat. Commun.* **8**, 1 (2017).
- [42] Nicolai Klemke, Nicolas Tancogne-Dejean, Giulio M. Rossi, Yudong Yang, F. Scheiba, R. E. Mainz, G. Di Sciacca, A. Rubio, F. X. Kärtner, and O. D. Mücke, Polarization-state-resolved high-harmonic spectroscopy of solids, *Nat. Commun.* **10**, 1 (2019).
- [43] Nariyuki Saito, Peiyu Xia, Faming Lu, Teruto Kanai, Jiro Itatani, and Nobuhisa Ishii, Observation of selection rules for circularly polarized fields in high-harmonic generation from a crystalline solid, *Optica* **4**, 1333 (2017).
- [44] Tobias Heinrich, Marco Taucher, Ofer Kfir, P. B. Corkum, André Staudte, Claus Ropers, and Murat Sivis, Chiral high-harmonic generation and spectroscopy on solid surfaces using polarization-tailored strong fields, *Nat. Commun.* **12**, 1 (2021).
- [45] Yong-Lin He, Jing Guo, Fang-Yan Gao, and Xue-Shen Liu, Dynamical symmetry and valley-selective circularly polarized high-harmonic generation in monolayer molybdenum disulfide, *Phys. Rev. B* **105**, 024305 (2022).
- [46] M. S. Mrudul, Álvaro Jiménez-Galán, Misha Ivanov, and Gopal Dixit, Light-induced valleytronics in pristine graphene, *Optica* **8**, 422 (2021).
- [47] M. S. Mrudul and G. Dixit, Controlling valley-polarisation in graphene via tailored light pulses, *J. Phys. B* **54**, 224001 (2021).
- [48] H. A. Hafez, S. Kovalev, J. C. Deinert, Z. Mics, B. Green, N. Awari, M. Chen, S. Germanskiy, U. Lehnert, and J. Teichert, *et al.*, Extremely efficient terahertz high-harmonic generation in graphene by hot Dirac fermions, *Nature* **561**, 507 (2018).
- [49] H. K. Avetissian and G. F. Mkrtchian, Impact of electron-electron Coulomb interaction on the high harmonic generation process in graphene, *Phys. Rev. B* **97**, 115454 (2018).
- [50] L. A. Chizhova, F. Libisch, and J. Burgdörfer, High-harmonic generation in graphene: Interband response and the harmonic cutoff, *Phys. Rev. B* **95**, 085436 (2017).
- [51] I. Al-Naib, J. E. Sipe, and M. M. Dignam, High harmonic generation in undoped graphene: Interplay of inter-and intraband dynamics, *Phys. Rev. B* **90**, 245423 (2014).
- [52] Ó. Zurrón, A. Picón, and L. Plaja, Theory of high-order harmonic generation for gapless graphene, *New J. Phys.* **20**, 053033 (2018).
- [53] Ó. Zurrón-Cifuentes, R. Boyero-García, C. Hernández-García, A. Picón, and L. Plaja, Optical anisotropy of non-perturbative high-order harmonic generation in gapless graphene, *Opt. Express* **27**, 7776 (2019).
- [54] M. Taucer, T. J. Hammond, P. B. Corkum, G. Vampa, C. Couture, N. Thiré, B. E. Schmidt, F. Légaré, H. Selvi, and N. Unsuree, *et al.*, Nonperturbative harmonic generation in graphene from intense midinfrared pulsed light, *Phys. Rev. B* **96**, 195420 (2017).
- [55] Z. Y. Chen and R. Qin, Circularly polarized extreme ultraviolet high harmonic generation in graphene, *Opt. Express* **27**, 3761 (2019).
- [56] Shunsuke A. Sato, Hideki Hirori, Yasuyuki Sanari, Yoshihiko Kanemitsu, and Angel Rubio, High-order

- harmonic generation in graphene: Nonlinear coupling of intraband and interband transitions, [Phys. Rev. B \*\*103\*\*, L041408 \(2021\)](#).
- [57] Roberto Boyero-García, Ana García-Cabrera, Oscar Zurrón-Cifuentes, Carlos Hernández-García, and Luis Plaja, Non-classical high harmonic generation in graphene driven by linearly-polarized laser pulses, [Opt. Express \*\*30\*\*, 15546 \(2022\)](#).
- [58] N. Yoshikawa, T. Tamaya, and K. Tanaka, High-harmonic generation in graphene enhanced by elliptically polarized light excitation, [Science \*\*356\*\*, 736 \(2017\)](#).
- [59] Yuntian Zhang, Liang Li, Jiapeng Li, Tengfei Huang, Pengfei Lan, and Peixiang Lu, Orientation dependence of high-order harmonic generation in graphene, [Phys. Rev. A \*\*104\*\*, 033110 \(2021\)](#).
- [60] C. Liu, Y. Zheng, Z. Zeng, and R. Li, Driving-laser ellipticity dependence of high-order harmonic generation in graphene, [Phys. Rev. A \*\*97\*\*, 063412 \(2018\)](#).
- [61] Fulong Dong, Qinzhi Xia, and Jie Liu, Ellipticity of the harmonic emission from graphene irradiated by a linearly polarized laser, [Phys. Rev. A \*\*104\*\*, 033119 \(2021\)](#).
- [62] M. S. Mrudul and Gopal Dixit, High-harmonic generation from monolayer and bilayer graphene, [Phys. Rev. B \*\*103\*\*, 094308 \(2021\)](#).
- [63] O. E. Alon, V. Averbukh, and N. Moiseyev, Selection Rules for the High Harmonic Generation Spectra, [Phys. Rev. Lett. \*\*80\*\*, 3743 \(1998\)](#).
- [64] T. Higuchi, C. Heide, K. Ullmann, H. B. Weber, and P. Hommelhoff, Light-field-driven currents in graphene, [Nature \*\*550\*\*, 224 \(2017\)](#).
- [65] Christian Heide, Takuya Higuchi, Heiko B. Weber, and Peter Hommelhoff, Coherent Electron Trajectory Control in Graphene, [Phys. Rev. Lett. \*\*121\*\*, 207401 \(2018\)](#).
- [66] Christian Heide, Yuki Kobayashi, Amalya C. Johnson, Fang Liu, Tony F. Heinz, David A. Reis, and Shambhu Ghimire, Probing electron-hole coherence in strongly driven 2D materials using high-harmonic generation, [Optica \*\*9\*\*, 512 \(2022\)](#).
- [67] Nicolai Klemke, O. D. Mücke, Angel Rubio, Franz X. Kärtner, and N. Tancogne-Dejean, Role of intraband dynamics in the generation of circularly polarized high harmonics from solids, [Phys. Rev. B \*\*102\*\*, 104308 \(2020\)](#).